Supplement to

Impact of HO_2/RO_2 ratio on highly oxygenated α-pinene photooxidation products and secondary organic aerosol formation potential

Yarê Baker et al.

Correspondence to: Thomas F. Mentel (t.mentel@fz-juelich.de)

S1 Sulfuric acid calibration for MION-APi-LTOF

The calibration source setup used by us was described in detail by KüRten et al. (2012) and was recently applied to a newer model of the MION chemical ionization inlet by He et al. (2023). In short H_2SO_4 is produced via the reaction of SO_2 with OH in a calibration source directly in front of the instrument. OH is produced via the photolysis of water from a humidified N_2 flow and the H_2SO_4 concentration is varied by variation of the humidified inflow.

The expected H_2SO_4 concentration is calculated with an open-source python library provided by Shen and He (2023). The model simulates the necessary gas phase chemistry based on a set of differential equations and uses two-dimensional convection-diffusion-reaction equations to take into account the losses of H_2SO_4 in the tubing. All that is needed for this calculation is the dimensions of the exact calibration setup. Details about the model can be found in He et al. (2023).

For the analyte signal we used the signal sum of the detected product ions HSO_4-, $H_2SO_4(NO_3)$- and $H_2SO_4(HNO_3NO_3)$- and normalized the signal with the sum of the NO_3- ion and (HNO_3NO_3)- cluster. The resulting calibration curve can be found in **Figure S1**. The calibration yielded a calibration factor of $7.0 \cdot 10^9$ molecules·cm^{-3}·ncps^{-1}, which is in the range of calibration factors reported before for different NO_3-MION inlets, for comparison see Rissanen et al. (2019) ($1.4 \cdot 10^9$ molecules·cm^{-3}·ncps^{-1}) and He et al. (2023) ($1.3 \cdot 10^{10}$ molecules·cm^{-3}·ncps^{-1}).

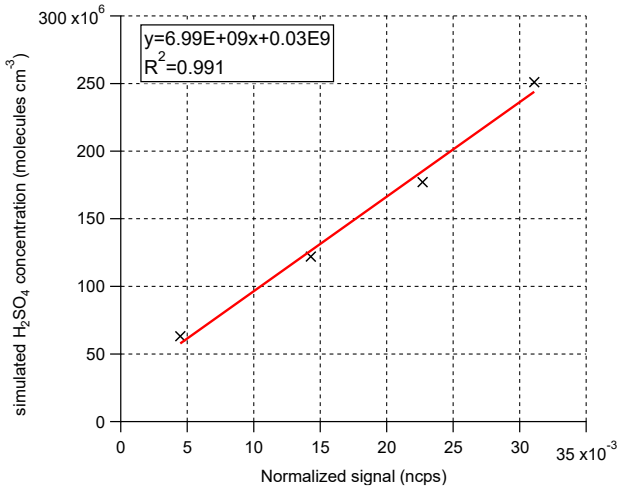

Figure S1: Calibration curve NO_3-MION-CIMS for H_2SO_4 calibration set-up

S2 Particle loss rate constant determination in SAPHIR STAR

The particle loss rate in the SAPHIR STAR chamber was determined by observation of the seed concentration decay in the chamber after stop of the particle addition. The exponential decay was fitted logarithmic as shown in **Eq. (S1)** and the lifetime $\tau_{Particle}$ ($k_{particleLoss} = \frac{1}{\tau_{Particle}}$) was determined. t is the time since start of the decay (time since seed addition stop) and τ and b are fitted for.

$$ln(normalized\ signal) = -\frac{1}{\tau} * t + b \quad \textbf{(S1)}$$

Exemplary the result of the fit for the total surface concentration measured in the SMPS is shown in **Figure S2**. The determination via AMS sulfate and ammonium signal as well as the number concentration measurement gave similar results. Therefore, the average determined particle lifetime in the chamber of 54 minutes was used. The residence time in the chamber was 63 minutes which shows that the seed particles are lost only slightly faster than the flush out rate due to some deposition.

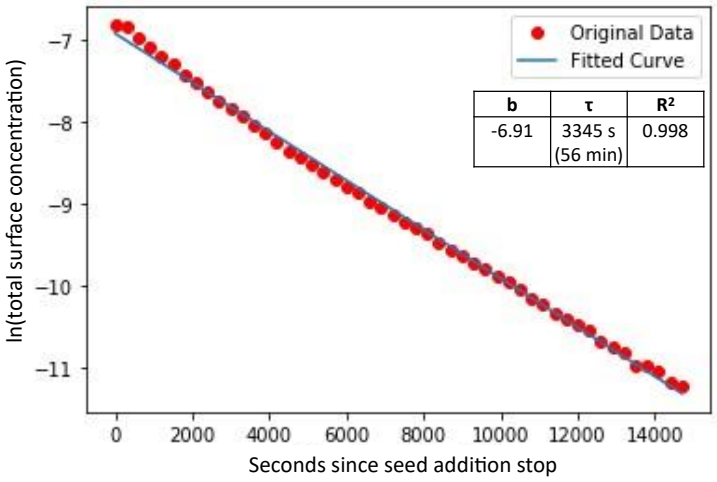

Figure S2: Logarithmic fit of particle surface decay timeseries to determine particle lifetime in the chamber

S3 Box model input parameters

The input parameters into the model are defined by the flows into the reactor and consist of the flows themselves, their humidity and the contained α-pinene, O_3 and CO concentration. Additional inputs are the temperature, pressure, and $J(O^1D)$. The UVC light is characterized by an on/off switch and the gap opening of the shielding. In separate experiments $J(O^1D)$ was calculated from O_3 loss as a function of the gap opening. Other necessary input parameters are the OH background reactivity (loss of OH without VOC present) and the wall loss of the RO_2 and HO_2 species in the STAR chamber. It is assumed that the product species in the MCM are too volatile to be lost on the walls, but that the radical species are lost upon wall collision. An OH background reactivity measurement (kOH instrument, see Lou et al. (2010), Fuchs et al. (2017) for more detailed information) was performed in the empty, very clean chamber at the same humidity as in the experiments. This yielded a reactivity of 3 s^{-1}. The background reactivity was adapted to represent the α-pinene consumption in the photooxidation phase correctly, resulting in a maximum $k_{OH\ Background} = 5\ s^{-1}$. A possible reason for the discrepancy is that the background reactivity determination was done in a very clean chamber while during the experiment series small residual contaminations, resisting flushing over > 6 residence times, may have contributed to the background reactivity.

For the estimation of the maximum wall loss the following experiment was performed twice: In a gas phase α-pinene photooxidation steady state the light was turned off and the decay of HOM product signals were observed in the NO_3-MION-CIMS. This approach was used before by Ehn et al. (2014) and Sarrafzadeh et al. (2016) to determine the maximum loss in the JPAC chamber.

Only products showing a clear single exponential decay were considered and it is assumed that the chosen HOMs are no longer produced after light off and lost on wall contact. Their timeseries is used to calculate an individual lifetime τ by fitting the decay curve to the function shown in **Eq. (S1)**. From the observation of the decay of C10 products an average lifetime of τ=171 s is determined.

The derived wall loss rate for HOM was also applied to describe the wall loss of RO_2 radicals, and therefore, $k_{RO_2\ wall}$ is set as 1/170 s^{-1}. The lifetime is correlated to the transport through the diffusion layer of the chamber thus should scale with the inverse of the square root of the molar mass (under the assumption of perfect mixing of the chamber core). It is therefore expected that the smaller HO_2 radical is lost faster due to its faster transport. Additionally, the removal efficiency for HO_2 and RO_2 radicals might differ further as RO_2 are not lost necessarily on every collision with the wall. The specific RO_2 removal efficiency depends on the radical's molecular structure (Miyazaki, 2012).

To estimate a value for the HO_2 wall loss, the expected diffusion constant for a HOM-Mon, HOM-Acc and HO_2 are calculated by the parametrization developed by Fuller et al. (1966) and recently reviewed by Tang et al. (2015). The results can be found in **Table S1**.

Table S1. **Calculated diffusion coefficients of an exemplary HOM-Mon, exemplary HOM-Acc and HO_2**

Compound	**Diffusion constant at 1 bar ($cm^2\ s^{-1}$)**
$C_{10}H_{15}O_6$ (HOM-Mon proxy)	0.053
$C_{20}H_{30}O_{10}$ (HOM-Acc proxy)	0.038
HO_2	0.202

If the wall loss is only dependent on the diffusion to the wall (i.e. 100 % loss on wall contact), the lifetime should inversely scale with the diffusion speed. To verify this assumption, the ratio of the average lifetimes of HOM-Mon and HOM-Acc were compared to the ratio of their diffusion constants: The HOM-Acc proxy's diffusion constant is 0.71 of the monomer proxy's diffusion constant. The observed accretion products decay resulted in average lifetime of τ=202 s, leading to $k_{HOM-Acc\ wall}$ / $k_{HOM-Mon\ wall}$ =0.85. Within the uncertainties of the diffusion constants calculation and the lifetime determination, the wall loss seems to depend indeed on the diffusion to the surface layer, thus on the diffusion constant. Therefore, considering the diffusion constant of HO_2, $k_{HO_2\ wall}$=1/50 s^{-1} is chosen.

To study the sensitivity of the modelled HO_2/RO_2 ratio to the assumed wall loss rates, a sensitivity study was performed by varying the rate coefficients for wall losses. The RO_2 wall loss was varied within 1σ of the determined HOM product wall loss. The HO_2 wall loss was varied in a wider range to cover the case that not all collision with the wall lead to loss of HO_2. Therefore, the lifetime of HO_2 was either set as 50 s or to a maximum lifetime of 170 s as determined by HOM monomer loss. The resulting HO_2/RO_2 ratios of the sensitivity study for the Exp1 experiment are displayed in **Table S2** as an example.

Table S2. Box model HO_2/RO_2 ratio results at varying RO_2 and HO_2 wall loss at low HO_2/RO_2 (left) and high HO_2/RO_2 (right in the Exp1 experiment

$\tau(HO_2)$ / $\tau(RO_2)$	low HO_2/RO_2		high HO_2/RO_2	
	50 s	***170 s***	***50 s***	***170 s***
145 s	6.8E-3	7.5E-3	0.7	1.0
170 s	6.4E-3	7.0E-3	0.6	0.9
195 s	6.1E-3	6.7E-3	0.6	0.9

The sensitivity study shows that independent of the assumed wall loss rate the HO2/RO2 ratio is around 0.007 and near one in the low and high HO2/RO2 case, respectively. In any case, the modelling results are only used to qualify the change of chemical regime and not to yield absolute values.

S4 Peaklist of oxidation products identified in NO_3-MION-CIMS

Table S3. Peaklist NO_3-MION-CIMS. All compounds were detected as clusters with $(NO_3)^-$. The table is sorted into fragments, monomers, and accretion products. Some compounds were just assignable in certain experiments, this is indicated by the superscript, no superscript indicated that the compound was assigned in all experiments.

Fragments		Monomers	Accretion products			
$C_5H_6O_4^{E1}$	$C_8H_{10}O_6$	$C_{10}H_{14}O_5$	$C_{14}H_{20}O_9$	$C_{17}H_{24}O_7$	$C_{19}H_{26}O_8^{E1,E2}$	$C_{20}H_{28}O_9$
$C_5H_6O_5$	$C_8H_{10}O_7$	$C_{10}H_{14}O_6$	$C_{14}H_{22}O_{10}$	$C_{17}H_{24}O_9$	$C_{19}H_{28}O_7$	$C_{20}H_{28}O_{11}$
$C_5H_6O_6$	$C_8H_{10}O_{10}^{E1}$	$C_{10}H_{14}O_7$	$C_{14}H_{22}O_{11}^{E1,E2}$	$C_{17}H_{24}O_{10}^{E1,E2}$	$C_{19}H_{28}O_8$	$C_{20}H_{30}O_6$
$C_5H_6O_7$	$C_8H_{12}O_5^{E1,E2}$	$C_{10}H_{14}O_8$	$C_{14}H_{26}O_{11}$	$C_{17}H_{24}O_{11}$	$C_{19}H_{28}O_9$	$C_{20}H_{30}O_7$
$C_5H_6O_8^{E2}$	$C_8H_{12}O_6$	$C_{10}H_{14}O_9$		$C_{17}H_{24}O_{13}^{E1,E2}$	$C_{19}H_{28}O_{10}$	$C_{20}H_{30}O_8$
$C_5H_7O_8$	$C_8H_{12}O_7$	$C_{10}H_{14}O_{10}$	$C_{15}H_{20}O_{14}^{E1}$	$C_{17}H_{26}O_8$	$C_{19}H_{28}O_{11}$	$C_{20}H_{30}O_9$
$C_5H_8O_7$	$C_8H_{12}O_8$	$C_{10}H_{14}O_{11}$	$C_{15}H_{22}O_9$	$C_{17}H_{26}O_9$	$C_{19}H_{28}O_{12}^{E1,E2}$	$C_{20}H_{30}O_{10}$
	$C_8H_{12}O_9$		$C_{15}H_{22}O_{10}$	$C_{17}H_{26}O_{10}$	$C_{19}H_{28}O_{13}$	$C_{20}H_{30}O_{11}$
$C_6H_6O_4^{E1,E3}$	$C_8H_{13}O_8$	$C_{10}H_{15}O_5$	$C_{15}H_{22}O_{11}$	$C_{17}H_{26}O_{11}$	$C_{19}H_{28}O_{14}^{E1,E2}$	$C_{20}H_{30}O_{12}$
$C_6H_{10}O_5$	$C_8H_{13}O_9$	$C_{10}H_{15}O_6$	$C_{15}H_{22}O_{12}^{E1,E2}$	$C_{17}H_{26}O_{12}$	$C_{19}H_{28}O_{15}^{E1}$	$C_{20}H_{30}O_{13}$
$C_6H_{10}O_6$	$C_8H_{14}O_5$	$C_{10}H_{15}O_7$	$C_{15}H_{22}O_{13}^{E1}$	$C_{17}H_{26}O_{13}^{E1,E2}$	$C_{19}H_{28}O_{16}^{E1,E2}$	$C_{20}H_{30}O_{14}$
$C_6H_{10}O_7$	$C_8H_{14}O_6$	$C_{10}H_{15}O_8$	$C_{15}H_{22}O_{14}^{E1}$	$C_{17}H_{26}O_{14}^{E1,E2}$	$C_{19}H_{30}O_6$	$C_{20}H_{30}O_{15}$
	$C_8H_{14}O_7$	$C_{10}H_{15}O_9$	$C_{15}H_{24}O_{13}^{E1,E2}$	$C_{17}H_{28}O_8$	$C_{19}H_{30}O_7$	$C_{20}H_{30}O_{16}$
$C_7H_8O_5^{E3}$	$C_8H_{14}O_8$	$C_{10}H_{15}O_{10}$	$C_{15}H_{26}O_{10}^{E1,E2}$	$C_{17}H_{28}O_9$	$C_{19}H_{30}O_8$	$C_{20}H_{30}O_{18}$
$C_7H_8O_6^{E3}$	$C_8H_{14}O_9$	$C_{10}H_{15}O_{11}$		$C_{17}H_{28}O_{10}$	$C_{19}H_{30}O_9$	$C_{20}H_{32}O_6$
$C_7H_8O_7$		$C_{10}H_{15}O_{12}$	$C_{16}H_{22}O_9^{E1,E2}$	$C_{17}H_{28}O_{11}$	$C_{19}H_{30}O_{10}$	$C_{20}H_{32}O_7$
$C_7H_8O_8$	$C_9H_{12}O_5$		$C_{16}H_{24}O_9$	$C_{17}H_{28}O_{12}$	$C_{19}H_{30}O_{11}$	$C_{20}H_{32}O_8$
$C_7H_{10}O_5^{E1,E3}$	$C_9H_{12}O_6$	$C_{10}H_{16}O_4$	$C_{16}H_{24}O_{10}$		$C_{19}H_{30}O_{12}$	$C_{20}H_{32}O_9$
$C_7H_{10}O_6$	$C_9H_{12}O_7$	$C_{10}H_{16}O_5$	$C_{16}H_{24}O_{11}$	$C_{18}H_{26}O_9$	$C_{19}H_{30}O_{13}$	$C_{20}H_{32}O_{10}$
$C_7H_{10}O_7$	$C_9H_{12}O_8$	$C_{10}H_{16}O_6$	$C_{16}H_{24}O_{12}^{E1,E2}$	$C_{18}H_{26}O_{10}$	$C_{19}H_{30}O_{14}^{E1,E2}$	$C_{20}H_{32}O_{11}$
$C_7H_{10}O_8$	$C_9H_{12}O_9$	$C_{10}H_{16}O_7$	$C_{16}H_{26}O_8$	$C_{18}H_{26}O_{11}$	$C_{19}H_{30}O_{15}^{E1,E2}$	$C_{20}H_{32}O_{12}$
$C_7H_{10}O_9^{E1,E2}$	$C_9H_{12}O_{12}^{E2}$	$C_{10}H_{16}O_8$	$C_{16}H_{26}O_9$	$C_{18}H_{26}O_{15}^{E1}$	$C_{19}H_{30}O_{16}^{E1}$	$C_{20}H_{32}O_{13}$
$C_7H_{10}O_{10}$	$C_9H_{13}O_9$	$C_{10}H_{16}O_9$	$C_{16}H_{26}O_{10}$	$C_{18}H_{28}O_6$	$C_{19}H_{32}O_7$	$C_{20}H_{32}O_{14}$
$C_7H_{14}O_5^{E1,E2}$	$C_9H_{13}O_{10}$	$C_{10}H_{16}O_{10}$	$C_{16}H_{26}O_{11}$	$C_{18}H_{28}O_8$	$C_{19}H_{32}O_8$	$C_{20}H_{32}O_{15}$
$C_7H_{14}O_6$	$C_9H_{14}O_4$	$C_{10}H_{16}O_{11}$	$C_{16}H_{26}O_{12}$	$C_{18}H_{28}O_9^{E1}$	$C_{19}H_{32}O_9$	$C_{20}H_{34}O_6$
	$C_9H_{14}O_5$		$C_{16}H_{26}O_{13}^{E2}$	$C_{18}H_{28}O_{10}$	$C_{19}H_{32}O_{10}$	$C_{20}H_{34}O_7$
	$C_9H_{14}O_6$	$C_{10}H_{17}O_6$	$C_{16}H_{28}O_{18}^{E1,E2}$	$C_{18}H_{28}O_{11}$	$C_{19}H_{32}O_{11}$	$C_{20}H_{34}O_8$
	$C_9H_{14}O_7$	$C_{10}H_{17}O_7$		$C_{18}H_{28}O_{12}^{E1,E2}$	$C_{19}H_{32}O_{12}$	$C_{20}H_{34}O_9$
	$C_9H_{14}O_8$	$C_{10}H_{17}O_8$		$C_{18}H_{28}O_{13}$	$C_{19}H_{32}O_{13}^{E1}$	$C_{20}H_{34}O_{10}$
	$C_9H_{14}O_9$	$C_{10}H_{17}O_9$		$C_{18}H_{28}O_{14}^{E1,E3}$	$C_{19}H_{32}O_{14}^{E1,E2}$	$C_{20}H_{34}O_{11}$
	$C_9H_{14}O_{10}$	$C_{10}H_{17}O_{10}^{E1,E3}$		$C_{18}H_{28}O_{15}^{E1}$	$C_{19}H_{32}O_7$	$C_{20}H_{34}O_{12}$
	$C_9H_{16}O_5$	$C_{10}H_{17}O_{11}^{E3}$		$C_{18}H_{28}O_{16}^{E1,E3}$	$C_{19}H_{32}O_8$	$C_{20}H_{34}O_{13}$
	$C_9H_{16}O_6$			$C_{18}H_{30}O_7$	$C_{19}H_{32}O_9$	
	$C_9H_{16}O_7$	$C_{10}H_{18}O_4$		$C_{18}H_{30}O_8$	$C_{19}H_{32}O_{10}$	
	$C_9H_{16}O_8$	$C_{10}H_{18}O_5$		$C_{18}H_{30}O_9$	$C_{19}H_{32}O_{11}$	
		$C_{10}H_{18}O_6$		$C_{18}H_{30}O_{10}$	$C_{19}H_{32}O_{12}$	
		$C_{10}H_{18}O_7$		$C_{18}H_{30}O_{11}$	$C_{19}H_{32}O_{13}^{E1,E3}$	
		$C_{10}H_{18}O_8$		$C_{18}H_{30}O_{12}$	$C_{19}H_{32}O_{14}^{E1,E2}$	
		$C_{10}H_{18}O_9$		$C_{18}H_{30}O_{13}$		
				$C_{18}H_{30}O_{14}^{E1}$		

S5 Estimation of change in peroxy radical steady state concentration between low and high HO_2/RO_2

Starting from the balance equation **Eq. (S2)**, we derived an equation for the steady state concentration (indicated by subscript SS) of an $[RO_2]_i$ (**Eq. (S3)**). The equations assume a primary production term Pri_i for $[RO_2]_i$, as well as only three significant loss pathways: The reaction with the pool of available $[RO_2]$ with a bulk reaction rate constant k_{RO2RO2}, the reaction with $[HO_2]$ with a reaction rate of $k_{RO2HO2}=1.85\cdot10^{-11}$ $cm^3\cdot s^{-1}$ at 20 °C as defined in the MCM (Jenkin et al., 1997; Saunders et al., 2003) and the wall loss. A wall loss rate coefficient of 1/170 s was used, as determined by our measurements for HOM products (see supplement section Fehler! Verweisquelle konnte nicht gefunden werden.). The rate coefficient k_{RO2RO2} was varied in a range $1.0\text{-}5.0\cdot10^{-12}$ $cm^3\cdot s^{-1}$, typical values expected for substituted organic peroxy radicals (Jenkin et al., 2019), to determine what bulk rate coefficient would be reconcilable with our observations. To compare directly to the measured ratio of HOM-RO_2 signal, we calculated the RO_2 concentration ratio at high to low HO_2/RO_2 applying **Eq. (S4)**. In **Eq. (S4)** the primary production term Pri_i could be eliminated as the primary production was same at high and low HO_2/RO_2 in our experiments.

$$\frac{d[RO_2]_i}{dt} = Pri_i - k_{RO2RO2}[RO_2][RO_2]_i - k_{HO2}[HO_2][RO_2]_i - k_{wall}[RO_2]_i \quad \textbf{(S2)}$$

$$[RO_2]_{i,SS} = \frac{Pri_i}{k_{RO2RO2}[RO_2] + k_{HO2}[HO_2] + k_{wall}} \quad \textbf{(S3)}$$

$$\frac{[RO_2]_{i,SS,highHO2}}{[RO_2]_{i,SS,lowHO2}} = \frac{k_{RO2RO2}[RO_2]_{SS,lowHO2} + k_{HO2}[HO_2]_{SS,lowHO2} + k_{wall}}{k_{RO2RO2}[RO_2]_{SS,highHO2} + k_{HO2}[HO_2]_{SS,highHO2} + k_{wall}} \quad \textbf{(S4)}$$

S6 Calculation of condensation rate constant k_{cond}

The condensation rate constant k_{cond} of each compound was calculated as shown in **Eq. (S5)**. Here α is the accommodation coefficient and is set to 1. $\bar{v}$ is the mean molecular speed calculated from the molar mass of the compound and S_{Ptot} is the total particle surface measured in the chamber. f_{FS} is the Fuchs-Sutugin factor which is calculated as shown in **Eq. (S6)**, where *knn* is the Knudsen Number calculated as shown in **Eq. (S7)**. $\bar{s}$ represents the mean free path of the molecule and p_{dia} the particle diameter. For p_{dia} we used the median diameter of the particle surface distribution measured (McFiggans et al., 2019).

$$k_{cond} = \alpha * f_{FS} * \frac{\bar{v}}{4} * S_{Ptot} \quad \textbf{(S5)}$$

$$f_{FS} = \frac{1 + knn}{1 + (0.75 * \frac{\alpha}{knn}) + knn + (0.283 * \alpha)} \quad \textbf{(S6)}$$

$$knn = \frac{2 * \bar{s}}{p_{dia}} \quad \textbf{(S7)}$$

S7 Error estimation via error propagation

Error propagation was utilized to estimate the error of derived parameters. For a parameter q, the error is defined by the errors of the variables $x,\ldots,z$ necessary to calculate q. The general equation to calculate the absolute uncertainty δq can be found in **Eq. (S8)**. This equation is only valid if the uncertainties in $x,\ldots,z$ are independent and random. (Taylor, 1997)

$$\delta q = \sqrt{\left(\frac{\partial q}{\partial x}\delta x\right)^2 + \ldots + \left(\frac{\partial q}{\partial z}\delta z\right)^2} \quad \textbf{(S8)}$$

For all measured parameters the measured standard deviation in steady state was used as the absolute uncertainty. For parameters that cannot be measured directly their uncertainties were calculated with error propagation as shown in **Eq. (S8)**. For the diffusion coefficient and the OH concentration we used uncertainties reported in the literature: Tang et al. (2015) reviewed diffusion coefficient calculation and came to the result that the difference between measurement and estimation via the method of Fuller et al. (1966) are mostly below 10 %. Therefore, we assumed a 10 % uncertainty for the diffusion coefficient of each formula composition. We assumed an uncertainty of 20 % for the OH concentration calculation as published by Wildt et al. (2014).

S8 Comparison of approximated (upper limit) HOM particulate mass concentration with measured organic mass

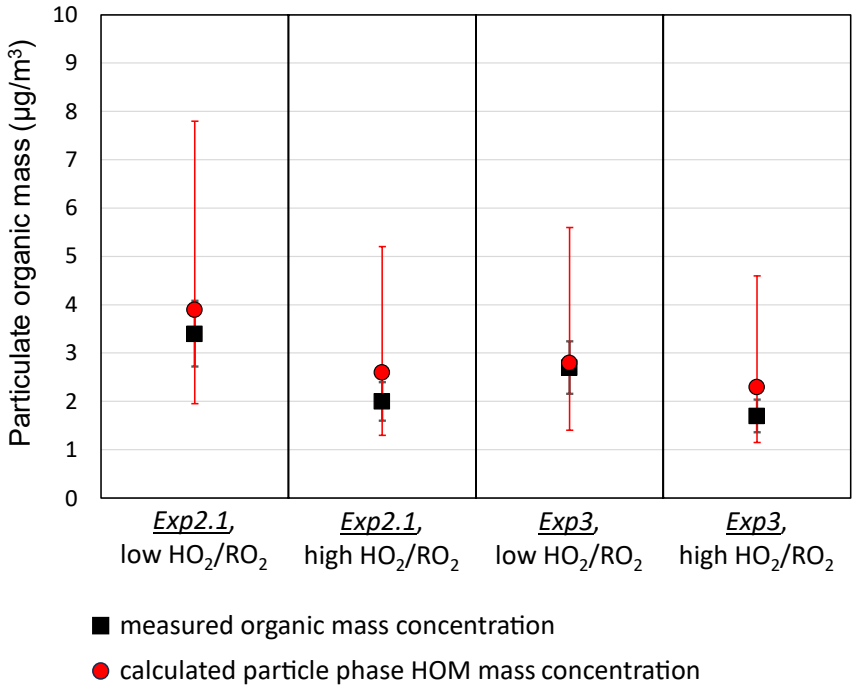

Figure S3: Comparison of particulate, organic mass concentration (measured by AMS) and approximation from NO_3-MION-CIMS measurements. Error of AMS measurement is estimated as 20 %. For calculated particle phase HOM mass concentration we assumed an uncertainty of factor 2 in the calibration factor (He et al., 2023).

References

Ehn, M., Thornton, J. A., Kleist, E., Sipila, M., Junninen, H., Pullinen, I., Springer, M., Rubach, F., Tillmann, R., Lee, B., Lopez-Hilfiker, F., Andres, S., Acir, I. H., Rissanen, M., Jokinen, T., Schobesberger, S., Kangasluoma, J., Kontkanen, J., Nieminen, T., Kurtén, T., Nielsen, L. B., Jorgensen, S., Kjaergaard, H. G., Canagaratna, M., Maso, M. D., Berndt, T., Petaja, T., Wahner, A., Kerminen, V. M., Kulmala, M., Worsnop, D. R., Wildt, J., and Mentel, T. F.: A large source of low-volatility secondary organic aerosol, Nature, 506, 476-479, https://doi.org/10.1038/nature13032, 2014.

Fuchs, H., Tan, Z. F., Lu, K. D., Bohn, B., Broch, S., Brown, S. S., Dong, H. B., Gomm, S., Häseler, R., He, L. Y., Hofzumahaus, A., Holland, F., Li, X., Liu, Y., Lu, S. H., Min, K. E., Rohrer, F., Shao, M., Wang, B. L., Wang, M., Wu, Y. S., Zeng, L. M., Zhang, Y. S., Wahner, A., and Zhang, Y. H.: OH reactivity at a rural site (Wangdu) in the North China Plain: contributions from OH reactants and experimental OH budget, Atmos. Chem. Phys., 17, 645-661, https://doi.org/10.5194/acp-17-645-2017, 2017.

Fuller, E. N., Schettler, P. D., and Giddings, J. C.: New method for prediction of binary gas-phase diffusion coefficients, Industrial & Engineering Chemistry, 58, 18-27, https://doi.org/10.1021/ie50677a007, 1966.

He, X.-C., Shen, J., Iyer, S., Juuti, P., Zhang, J., Koirala, M., Kytökari, M. M., Worsnop, D. R., Rissanen, M., Kulmala, M., Maier, N. M., Mikkilä, J., Sipilä, M., and Kangasluoma, J.: Characterisation of gaseous iodine species detection using the multi-scheme chemical ionisation inlet 2 with bromide and nitrate chemical ionisation methods, Atmos. Meas. Tech., 16, 4461-4487, https://doi.org/10.5194/amt-16-4461-2023, 2023.

Jenkin, M. E., Saunders, S. M., and Pilling, M. J.: The tropospheric degradation of volatile organic compounds: a protocol for mechanism development, Atmos. Environ., 31, 81-104, https://doi.org/10.1016/S1352-2310(96)00105-7, 1997.

Jenkin, M. E., Valorso, R., Aumont, B., and Rickard, A. R.: Estimation of rate coefficients and branching ratios for reactions of organic peroxy radicals for use in automated mechanism construction, Atmos. Chem. Phys., 19, 7691-7717, https://doi.org/10.5194/acp-19-7691-2019, 2019.

Kürten, A., Rondo, L., Ehrhart, S., and Curtius, J.: Calibration of a chemical ionization mass spectrometer for the measurement of gaseous sulfuric acid, J. Phys. Chem. A, 116, 6375-6386, https://doi.org/10.1021/jp212123n, 2012.

Lou, S., Holland, F., Rohrer, F., Lu, K., Bohn, B., Brauers, T., Chang, C. C., Fuchs, H., Häseler, R., Kita, K., Kondo, Y., Li, X., Shao, M., Zeng, L., Wahner, A., Zhang, Y., Wang, W., and Hofzumahaus, A.: Atmospheric OH reactivities in the Pearl River Delta - China in summer 2006: measurement and model results, Atmos. Chem. Phys., 10, 11243-11260, https://doi.org/10.5194/acp-10-11243-2010, 2010.

McFiggans, G., Mentel, T. F., Wildt, J., Pullinen, I., Kang, S., Kleist, E., Schmitt, S., Springer, M., Tillmann, R., Wu, C., Zhao, D., Hallquist, M., Faxon, C., Le Breton, M., Hallquist, A. M., Simpson, D., Bergstrom, R., Jenkin, M. E., Ehn, M., Thornton, J. A., Alfarra, M. R., Bannan, T. J., Percival, C. J., Priestley, M., Topping, D., and Kiendler-Scharr, A.: Secondary organic aerosol reduced by mixture of atmospheric vapours, Nature, 565, 587-593, https://doi.org/10.1038/s41586-018-0871-y, 2019.

Miyazaki, K.: Study of the nature and roles of peroxy radicals in the atmosphere towards the understanding of oxidant formation using laser-flash photolysis and LIF detection technique, Tokyo Metropolitan University; University of Lille, 2012.

Rissanen, M. P., Mikkilä, J., Iyer, S., and Hakala, J.: Multi-scheme chemical ionization inlet (MION) for fast switching of reagent ion chemistry in atmospheric pressure chemical ionization mass spectrometry (CIMS) applications, Atmos. Meas. Tech., 12, 6635-6646, https://doi.org/10.5194/amt-12-6635-2019, 2019.

Sarrafzadeh, M., Wildt, J., Pullinen, I., Springer, M., Kleist, E., Tillmann, R., Schmitt, S. H., Wu, C., Mentel, T. F., and Zhao, D.: Impact of NO x and OH on secondary organic aerosol formation from β-pinene photooxidation, Atmospheric chemistry and physics, 16, 11237-11248, 2016.

Saunders, S. M., Jenkin, M. E., Derwent, R., and Pilling, M.: Protocol for the development of the Master Chemical Mechanism, MCM v3 (Part A): tropospheric degradation of non-aromatic volatile organic compounds, Atmos. Chem. Phys., 3, 161-180, https://doi.org/10.5194/acp-3-161-2003, 2003.

Shen, J. and He, X.-C.: MARFORCE-Flowtube model, https://github.com/momo-catcat/MARFORCE-flowtube [code], https://doi.org/10.5281/zenodo.8318790, 2023.

Tang, M., Shiraiwa, M., Pöschl, U., Cox, R., and Kalberer, M.: Compilation and evaluation of gas phase diffusion coefficients of reactive trace gases in the atmosphere: Volume 2. Diffusivities of organic compounds, pressure-normalised

mean free paths, and average Knudsen numbers for gas uptake calculations, Atmos. Chem. Phys., 15, 5585-5598, https://doi.org/10.5194/acp-15-5585-2015, 2015.
Taylor, J.: Introduction to error analysis, the study of uncertainties in physical measurements, 1997.
Wildt, J., Mentel, T. F., Kiendler-Scharr, A., Hoffmann, T., Andres, S., Ehn, M., Kleist, E., Müsgen, P., Rohrer, F., Rudich, Y., Springer, M., Tillmann, R., and Wahner, A.: Suppression of new particle formation from monoterpene oxidation by NOx, Atmos. Chem. Phys., 14, 2789-2804, https://doi.org/10.5194/acp-14-2789-2014, 2014.